Talanta 141 (2015) 66–72

Contents lists available at ScienceDirect

Talanta

journal homepage: www.elsevier.com/locate/talanta

A glucose biosensor based on partially unzipped carbon nanotubes

Huifang Hu, Miao Feng, Hongbing Zhan *

College of Materials Science and Engineering, Fuzhou University, Fuzhou 350116, China

ARTICLE INFO

Article history:
Received 13 January 2015
Received in revised form
22 March 2015
Accepted 25 March 2015
Available online 2 April 2015

Keywords:
Partially unzipped carbon nanotubes
Glucose oxidase
Glucose
Biosensor

ABSTRACT

An amperometric glucose biosensor based on direct electron transfer of glucose oxidase (GOD) self-assembled on the surface of partially unzipped carbon nanotubes (PUCNTs) modified glassy carbon electrode (GCE) has been successfully fabricated. PUCNTs were synthesized via a facile chemical oxidative etching CNTs and used as a novel immobilization matrix for GOD. The cyclic voltammetric result of the PUCNT/GOD/GCE showed a pair of well-defined and quasi-reversible redox peaks with a formal potential of −0.470 V and a peak to peak separation of 37 mV, revealing that the fast direct electron transfer between GOD and the electrode has been achieved. It is notable that the glucose determination has been achieved in mediator-free condition. The developed biosensor displayed satisfactory analytical performance toward glucose including high sensitivity (19.50 $\mu A\,mM^{-1}\,cm^{-2}$), low apparent Michaelis–Menten (5.09 mM), a wide linear range of 0–17 mM, and also preventing the interference from ascorbic acid, uric acid and dopamine usually coexisting with glucose in human blood. In addition, the biosensor acquired excellent storage stabilities. This facile, fast, environment-friendly and economical preparation strategy of PUCNT–GOD may provide a new platform for the fabrication of biocompatible glucose biosensors and other types of biosensors.

1. Introduction

Partially unzipped carbon nanotubes (PUCNTs), as seamless junctions between 1-dimensional CNTs and 2-dimensional graphene [1], have attracted enormous interest from both theoretical and experimental scientists. Because of their distinctive structural features, PUCNTs display unique electrical [2–5], thermal [6], magnetic [7,8], optical [9] and mechanical [10,11] properties that are quite different from those of CNTs and graphene. Considerable experimental efforts have been dedicated to realize the practical application of PUCNTs in devices such as photodetectors, field-effect transistors [8], magnetic field sensors [12], biosensors [13] and as catalyst support for proton exchange membrane fuel cells [14].

PUCNTs show a graphene-like structure on their outer walls, while retaining a partially tubular structure (from the parent CNTs) on their inner walls. With a certain degree of unzipping, the CNT outer walls are partly unzipped, leaving a large number of small graphene pieces attached to the inner walls. These structures present abundant edges and defect sites, which are responsible for electrochemical activity and other types of activity [15–20]. The less damaged (or intact) inner walls of the CNTs are highly stable, and maintain their high electrical conductivity in the complex; this electrical conductivity is needed to sustain efficient charge transport during electrochemical processes [21–23]. This material has been identified as a promising electrode for high-capacitance supercapacitors, which can yield a specific capacitance of an order of magnitude greater than that of untreated multiwall carbon nanotubes (MWCNTs) [24,25]. PUCNTs can also be used as cathode materials for lithium–air batteries; the PUCNTs can intertwine with each other to form a tridimensional porous film, and they exhibit almost twice the discharge capacity of raw CNTs. PUCNTs have similar characteristics to graphene in terms of their O_2 chemisorption properties, which lead to higher oxygen reduction reactivity [26,27]. Further, PUCNTs are comparable with graphene at all charging/discharging current densities. Research into electrochemical biosensors revealed that PUCNTs exhibit extraordinary electrochemical properties, with superior oxidation currents and lower limits of detection toward analytes, compared with MWCNTs and graphene [13,28]. Our previous work also highlighted the superior fundamental electrochemical properties of PUCNTs [29,30].

To date, most research into glucose biosensors has focused either on CNTs [31,32] or graphene [33–35]. In contrast, little is known about glucose biosensors that integrating both of these materials. Mani et al. [36] synthesized graphene oxide (GO)–MWCNT hybrid materials by sonicating a dispersion of GO and MWCNTs in liquid. The GO–MWCNT material was then electrochemically reduced on a glassy carbon electrode (GCE) to obtain electrochemically reduced

* Corresponding author. Tel.: +86 591 22866532; fax: +86 591 22866539.
E-mail address: hbzhan@fzu.edu.cn (H. Zhan).

http://dx.doi.org/10.1016/j.talanta.2015.03.057
0039-9140/

GO (ERGO)–MWCNT. The ERGO–MWCNT-modified-GCE exhibited high electrocatalytic activity toward glucose in the presence of oxygen and the mediator ferrocene mono-carboxylic acid (FMCA). Hwa et al. [37] also obtained GO–CNT materials, via ultrasonication and heating with zinc acetate and $NaBH_4$ for a number of hours, which yielded graphene–CNT–ZnO. The GCE modified with a graphene–CNT–ZnO film revealed high electrocatalytic ability for the detection of glucose in the presence of oxygen, along with appreciable repeatability, good reproducibility and remarkable stability. Both of these studies achieved some progress over previous work; however, these studies were limited by inherent disadvantages of the materials used. The hybrids were a simple mixture of pre-synthesized CNTs and graphene. The interaction between GO and CNTs is a non-covalent π–π stacking interaction, which is a weak coupling. The preparation of GCEs is a time-consuming and high-cost method that involves several steps. Therefore, a simple, low-cost and stable method to fabricate GCEs is highly desired.

In this work, we synthesized PUCNTs with a hybrid structure combining pristine CNTs and curved graphene sheets, via a facile chemical oxidative etching process. The graphene, with its large surface area, provided sufficient anchoring sites for the immobilization of various inorganic and organic catalyst particles, and the original MWCNTs on the inside of the hybrid material preserved their excellent conductivity. GCEs modified with PUCNTs were successfully utilized to immobilize GOD, and this modified GCE was used as a glucose biosensor. The sensor developed here showed high sensitivity, required only simple fabrication processes and was low-cost.

2. Experimental methods

2.1. Materials and reagents

MWCNTs (purity $>97\%$, ca. 20 nm in diameter and 5–15 μm in length) were purchased from Shenzhen Nanotech Port Co. Ltd. (Shenzhen China). Ascorbic acid (AA), uric acid (UA), dopamine (DA), D-glucose, 1-ethyl-3-(3-dimethylaminopropyl) carbodiimide hydrochloride (EDC), and N-hydroxy-sulfosuccinimide (NHS) were purchased from Aladdin Ltd. (Shanghai, China). Glucose oxidase (GOD) was purchased from Sigma-Aldrich Co., Llc., USA. All other reagents were purchased from Sinopharm Chemical Reagent Co. Ltd. (Shanghai, China) and were reagent grade. Deionized-ultrafiltered ($>18.25\ M\Omega\ cm^{-1}$) water was used to prepare all aqueous solutions.

2.2. Apparatus and measurements

Transmission electron microscopy (TEM) images were obtained using a Tecnai G2F20 S-TWINfield emission transmission electron microscope. Surface morphologies and structures of the samples were observed by scanning electron microscopy (SEM, Supra-55, Zeiss, Inc.). All electrochemical experiments were performed in an electrochemical workstation (CHI 660E, Shanghai Chenhua Instrument Co. Ltd., China) on a conventional three-electrode system with a saturated calomel electrode (SCE) as the reference electrode, a platinum wire as the auxiliary electrode, and GCE ($Ø=3$ mm) as the working electrode. Electrochemical impedance spectroscopy (EIS) was carried out in 5 mM $K_3[Fe(CN)_6]/K_4[Fe(CN)_6]$ with 0.1 M KCl in the frequency range from 100 kHz to 0.1 Hz.

2.3. Synthesis of PUCNTs

PUCNTs were synthesized according to Tour's method [38]. Briefly, MWCNTs (150 mg) were dispersed in concentrated H_2SO_4 (36 mL) and H_3PO_4 (4 mL). The dispersion was then treated with $KMnO_4$ (450 mg) at 25 °C for 1 h and then heated to 65 °C for an additional 2 h. After cooling to room temperature, the mixture was washed with deionized-ultrafiltered water until the pH was neutral.

2.4. Preparation of the electrode

The GCE was polished using 1.0 μm, 0.5 μm and 0.05 μm alumina powder and was then sonicated with ethanol and deionized-ultrafiltered water for 5 min, respectively. The GCE was then dried.

Next, 8 μL of an aqueous dispersion of PUCNTs (1 mg/mL) was cast on the pretreated GCE surface and then allowed to dry in air, yielding a PUCNT/GCE. The electrode was then immersed in 0.1 M PBS (pH5.8) containing 10 mM EDC and 100 mM NHS for 3 h to activate the carboxylic groups in the PUCNTs [39]. The electrode was then washed with PBS (pH7.0), and immediately immersed in a GOD solution (10 mg/mL) for 12 h. Finally, the electrode was gently washed with PBS (pH7.0), and dried for 24 h at 4 °C. The prepared enzyme electrode was stored at 4 °C when not in use. The same procedure was employed to fabricate a GOD/GCE and MWCNT/GOD/GCE.

3. Results and discussion

3.1. Characterization of the PUCNT modified electrode

The morphology of the PUCNTs was characterized using TEM. Fig. 1A shows a TEM image of the PUCNTs, which revealed that the outer layers of the original MWCNTs were successfully exfoliated during the unzipping process, and the primitive structure of the MWCNTs was maintained in the inner structure of the hybrid material. Fig. 1B shows that the PUCNTs had a junction structure, with an outer graphene portion, and an inner CNT portion. The morphology of PUCNTs and the PUCNT/GOD on the GCE surface were studied using SEM. Fig 1C shows that the edges of the PUCNTs were rough, providing sufficient anchoring sites for the immobilization of enzymes; the three dimensional, multi-pore, layered PUCNT film produced here was beneficial for the mass transfer. After self-assembly of the GOD, the PUCNT/GOD formed a homogenous, mushy film (Fig. 1D), suggesting that the GOD was successfully attached on the surface of the PUCNT/GCE.

EIS is a powerful technique that was applied to obtain information about the changes in impedance that resulted from changes in the electrode surface during the modification process. Fig. 2A shows EIS spectra for the bare GCE (a), PUCNT/GCE (b), GOD/GCE (c), PUCNT/GOD/GCE (d), MWCNT/GCE (e), and MWCNT/GOD/GCE (f) in a 5.0 mM $Fe(CN)_6^{3-}/Fe(CN)_6^{4-}$ solution containing 0.1 M KCl. The Randles equivalent circuit model was used to fit the experimental data, where R_{ct} is the charge transfer resistance, R_s is the electrolyte resistance, Z_w is the Warburg impedance and C_{dl} is the double layer capacitance (Fig. 2A, below inset). The diameter of the semicircle described by the plot indicated the magnitude of R_{ct}, and the substantially semicircular portion of the plot corresponded to the electron transfer-limited process; the straight-line portion of the plot corresponded to the diffusion-limited process. The EIS of the bare GCE displayed a small semicircle, implying a low R_{ct} (60 Ω) toward the redox probe $Fe(CN)_6^{3-/4-}$. The R_{ct} of the MWCNT/GCE (100 Ω) was larger than that of bare GCE. However, for the GCE modified with PUCNTs, the R_{ct} value decreased to 80 Ω. This suggested that the PUCNTs retained the high conductivity of the CNTs and achieved the abundant surface defects from the outer graphene sheets [1]. The interpenetrating network formed by the PUCNTs was favorable for redox probes, and for interfacial electron transfer on the GCE surface. When GOD was coated on the GCE, the R_{ct} value for GOD/GCE dramatically increased to 5000 Ω, suggesting that the GOD generated an

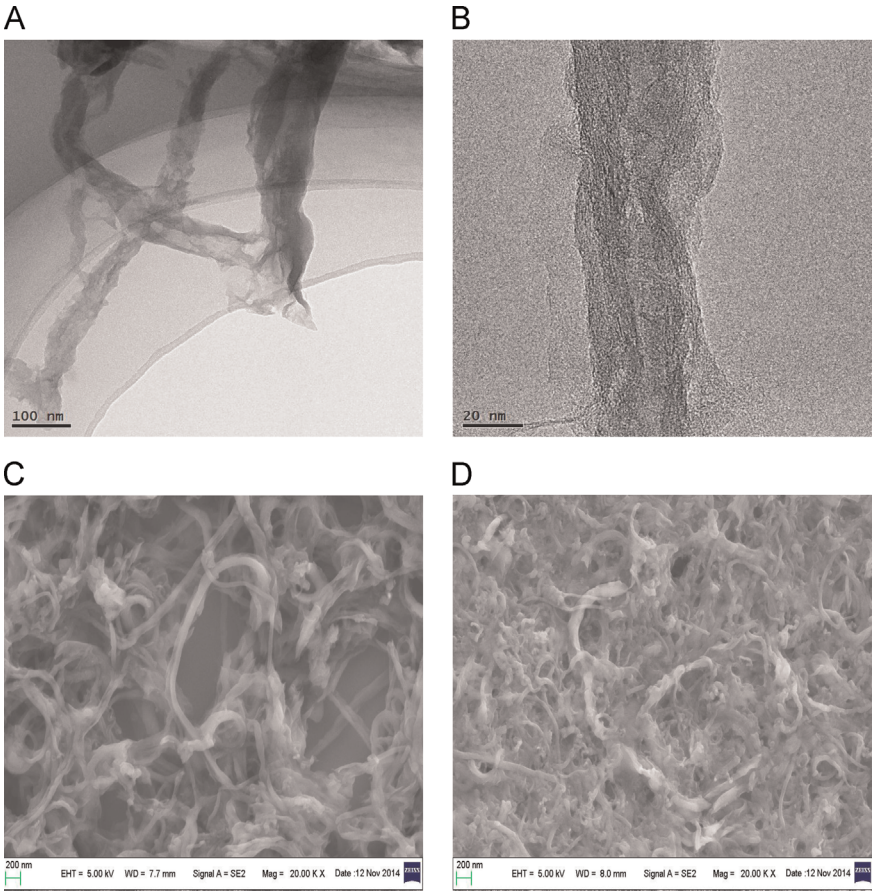

Fig.1. (A) Typical and (B) high-resolution TEM images of PUCNTs; SEM images of PUCNT/GCE (C) and PUCNT/GOD/GCE (D).

insulating layer on the electrode surface that blocked the electronic charge transfer [40]. When PUCNTs were added to the enzyme, the R_{ct} value (2500 Ω) was much smaller than that obtained for the GOD/GCE, also smaller than CNT/GOD/GCE (3000 Ω). This result indicated that the GOD had been successfully immobilized on the surface of the PUCNTs, and PUCNT/GOD/GCE had the fastest electron transfer. The surface coverage of GOD (θ_E) on the electrode modified by PUCNTs was calculated to be 94.1%, according to the equation $\theta_E = (1-R_{ct}/R_{ct}^{GOD}) \times 100\%$ [41], indicating that the PUCNT film had superior capabilities for immobilization of large quantities of enzymes on the electrode surface.

Cyclic voltammetry (CV) measurements were performed using the bare GCE (a), the PUCNT/GCE (b) and the MWCNT/GCE (c); the measurements were conducted in a 5.0 mM $Fe(CN)_6^{3-/4-}$ solution containing 0.1 M KCl at scan rate of 100 mV s^{-1} as shown in Fig. 2B. Compared with the bare GCE and the MWCNT/GCE, the PUCNT/GCE exhibited a smaller peak-to-peak separation (ΔE_p) and a higher peak current, which illustrated the fast electron-transfer kinetics of the PUCNT/GCE. When the scan rate increased, the redox potentials shifted slightly, and the peak currents increased. The anodic peak current (*I*pa) and the cathodic peak current (*I*pc) for the PUCNT/GCE showed a linear relationship with the square-root of the scan rate, for scan rates from 25 to 500 mV s^{-1} (Fig. 2B, inset). The results indicated that the action was a diffusion-controlled, reversible electrochemical reaction.

3.2. Direct electrochemistry of GOD immobilized in the PUCNT film

To investigate the electrochemical properties of the PUCNT/GOD/GCE, CVs were employed to evaluate the different electrodes. Fig. 3A shows the CVs obtained at the bare GCE (a), GOD/GCE (b), PUCNT/GOD/GCE (c), and MWCNT/GOD/GCE (d) in 0.1 M PBS at scan rate of 100 mV s^{-1}. No redox peaks were observed at the bare GCE and the GOD/GCE, revealing that they were electrochemically silent in this potential window. Redox peaks at the CV of MWCNT/GOD/GCE were hardly observed, which was due to the inert side wall and few available active sites of the MWCNTs that inhibited the direct electron transfer between GOD and GCE. In contrast, the CV for the PUCNT/GOD/GCE showed a pair of well-defined and quasi-reversible peaks at −0.488 and −0.451 V, with a ΔE_p of 37 mV at 100 mV s^{-1}. This low ΔE_p value revealed a fast electron transfer process. The formal potential ($E^{\circ\prime}$) for the redox couple is −0.470 V, which was close to the $E^{\circ\prime}$ values reported previously for GOD [40,42]. The redox peaks for PUCNT/GOD/GCE were attributed to the direct electron transfer of GOD for the conversion of GOD (FAD) and GOD ($FADH_2$), suggesting that the direct electrochemistry of the GOD self-assembled on the PUCNTs was achieved. The GOD undergoes a redox reaction, as follows [43]:

$$\text{GOD–FAD} + 2e^- + 2H^+ \leftrightarrow \text{GOD–FADH}_2 \quad (1)$$

The surface coverage (Γ) of the PUCNT/GOD/GCE with the electro-active enzyme was estimated from the integration of the anodic and cathodic peaks of the CVs. Γ was calculated to be 5.22×10^{-11} mol cm^{-2} at 100 mV s^{-1}, using the equation $\Gamma = Q/nFA$ [44], where Q is the charge involved in the reaction, n is the number of electrons transferred ($n=2$), F is the Faraday constant ($F=96{,}485.34$ C mol^{-1}), and A is the geometric area of the working electrode (0.07 cm^2). This value was much larger than those of 2.86×10^{-12} mol cm^{-2} for the monolayer of GOD deposited on the bare GCE [45], 3.32×10^{-11} mol cm^{-2} at TCS–TiO_2/GOD/chitosan/GCE [43] and 1.43×10^{-11} mol cm^{-2} at In_2O_3/chitosan/GOD/GCE [46], indicating that GOD had achieved a multilayered and

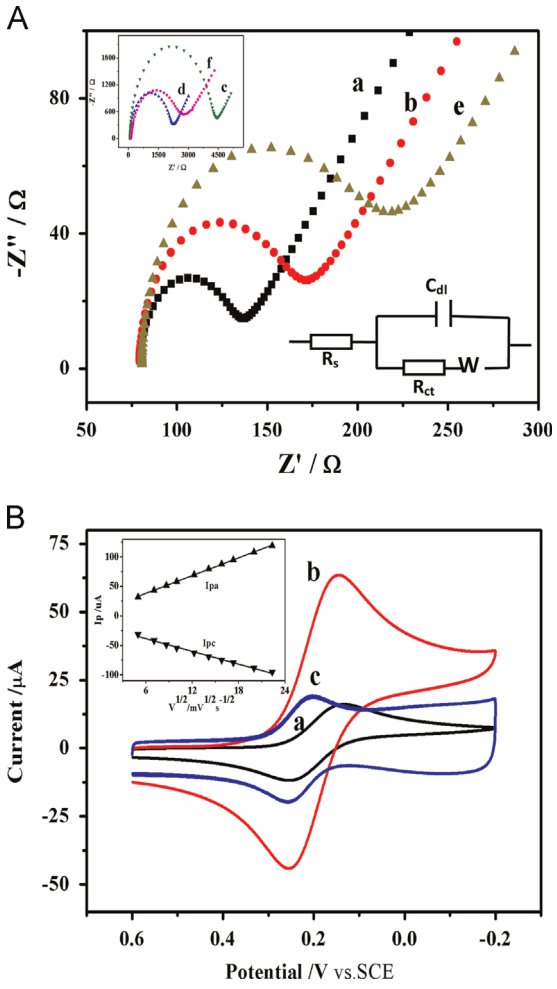

Fig. 2. (A) EIS for bare GCE (a), PUCNT/GCE (b), GOD/GCE (c), PUCNT/GOD/GCE (d), MWCNT/GCE (e), MWCNT/GOD/GCE (f) in 5.0 mM $Fe(CN)_6^{3-/4-}$ (1:1) solution containing 0.1 M KCl. (B) CVs of bare GCE (a), PUCNT/GCE (b) and MWCNT/GCE (c) in 5.0 mM $Fe(CN)_6^{3-/4-}$ (1:1) solution containing 0.1 M KCl; Scan rate: 100 mV s^{-1}. The inset is peak current dependence on the square-root of scan rate at PUCNT/GCE.

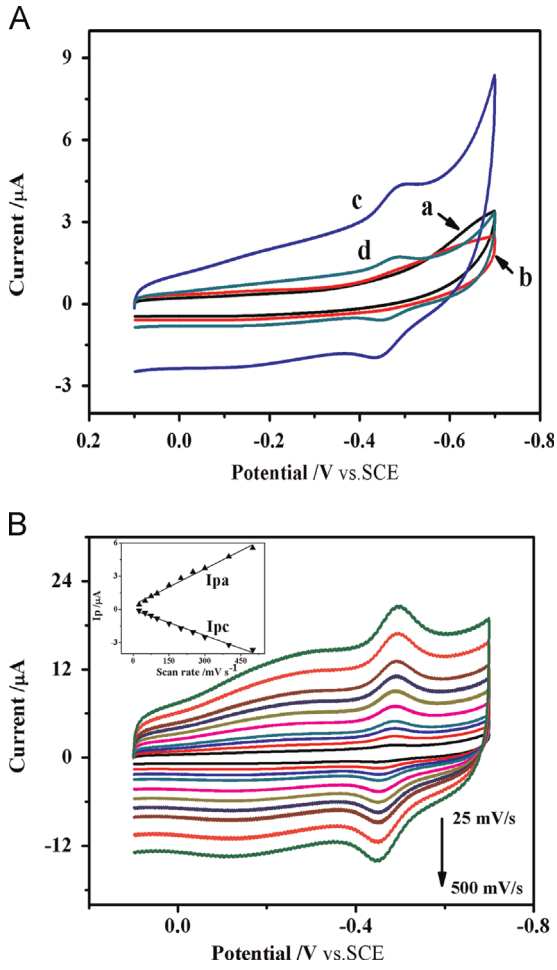

Fig. 3. (A) CVs of bare GCE (a), GOD/GCE (b), PUCNT/GOD/GCE (c), and MWCNT/GOD/GCE (d) in N_2-saturated PBS solution (0.1 M, pH7.0); Scan rate: 100 mV s^{-1}. (B) CVs of PUCNT/GOD/GCE in N_2-saturated PBS solution (0.1 M, pH7.0) at different scan rates: 25, 50, 75, 100, 150, 200, 250, 300, 400, and 500 mV s^{-1}. The inset is the plot of peak currents vs. scan rates.

three-dimensional coverage of the PUCNTs. This result proved that the high surface area and good biocompatibility of the PUCNTs facilitated high levels of enzyme loading, and increased the surface area of the PUCNT/GOD/GCE.

To evaluate the reversible electron transfer phenomenon in more detail, CVs were recorded for the PUCNT/GOD/GCE at different scan rates in PBS (pH7.0), under N_2-saturated conditions (Fig. 3B). As shown in Fig. 3B, the ratio of Ipa and Ipc for the PUCNT/GOD/GCE was almost identical. Ipa and Ipc increased linearly with the increases in the scan rate, with correlation coefficient (R^2) values of 0.987 and 0.988 for *I*pa and *I*pc, respectively, in the scan rate range of 25–500 mV s^{-1} (shown in the inset in Fig. 3B). This result indicated that the electrode transfer between GOD and GCE occurred easily at the PUCNT/GOD composite film, and the transfer behavior was characteristic of a surface-confined electrode process, not a diffusion-controlled process.

3.3. Performance of PUCNT/GOD/GCE based glucose biosensor

In order to investigate the enzymatic activity of the GOD immobilized on the modified electrode, further bio-electrocatalytic experiments investigating the reaction of oxygen and glucose to the GOD were carried out. CVs were measured for GOD/GCE and PUCNT/GCE in N_2-saturated and O_2-saturated (without and with glucose) solutions, as control experiments. No peak was observed for the GOD/GCE (Fig. 4A). This was because the activity center of GOD is deeply buried in a protective shell, and it was therefore difficult for direct electron transfer to occur between the GOD and the electrode. Similarly, no peaks were observed in the CVs for the PUCNT/GCE, because of the complete lack of catalytic activity of the PUCNT toward glucose. Fig. 4C shows CVs for the PUCNT/GOD/GCE in a N_2-saturated PBS solution (a), an O_2-saturated PBS solution (b), and an O_2-saturated PBS solution containing 2 mM glucose (c), measured at a scan rate of 100 mV s^{-1}. Compared with curve a (for the N_2-saturated PBS), an enhancement in the reduction peak current was observed in the presence of O_2, with a decrease in the oxidation peak current (Fig 4C, curve b). These changes demonstrated that the GOD in the film catalyzed the oxygen reduction well, in accordance with Eqs. (1) and (2) [43]. Furthermore, as a result of the addition of 2 mM of glucose to the O_2-saturated solution, the reduction peak current decreased (Fig 4C, curve c). The reduction current decreased as the glucose concentration was increased (Fig. 4D). This phenomenon was attributed to the enzyme-catalyzed glucose oxidation described by Eq. (3).

$$GOD\text{–}FADH_2 + O_2 \rightarrow GOD\text{–}FAD + H_2O_2 \quad (2)$$

$$Glucose + GOD\text{–}FAD \rightarrow GOD\text{–}FADH_2 + gluconolactone \quad (3)$$

To further illustrate the relationship between the electro-catalytic redox current and the concentration of glucose, differential

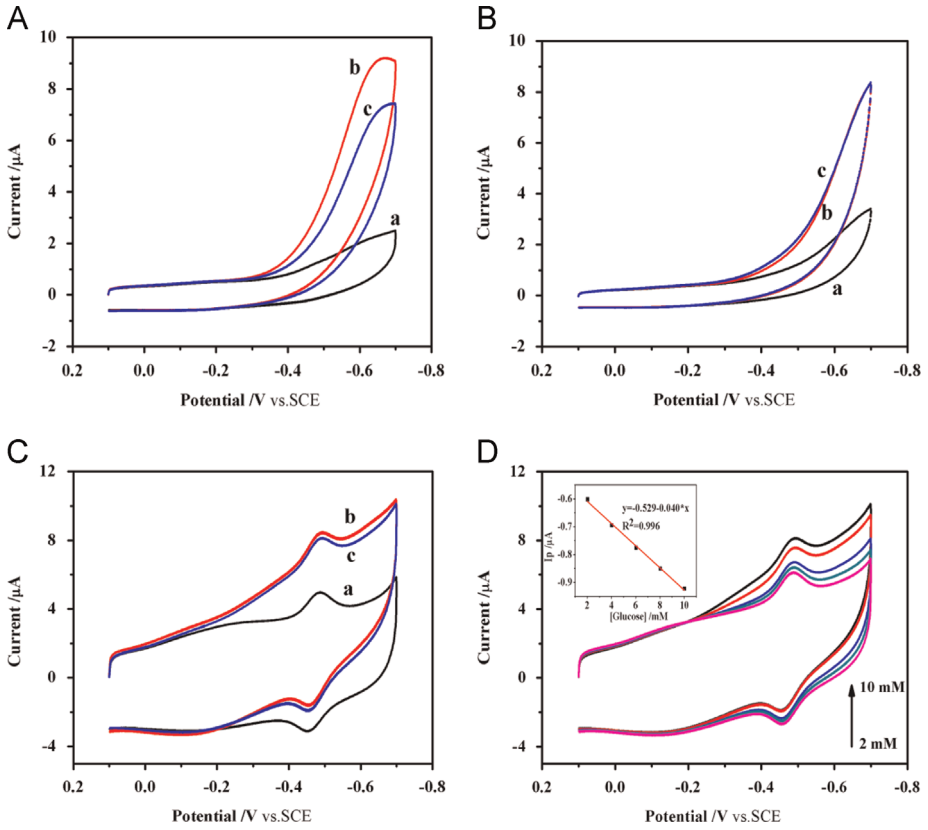

Fig. 4. CVs of GOD/GCE (A), PUCNT/GCE (B) and PUCNT/GOD/GCE (C) in N_2-saturated (a), O_2-saturated PBS solution (0.1 M, pH7.0) in the absence (b) and presence of 2 mM glucose (c); scan rate: 100 mV s^{-1}. (D) CVs of PUCNT/GOD/GCE in O_2-saturated PBS solution in various concentrations of the glucose: 2, 4, 6, 8, and 10 mM; scan rate: 100 mV s^{-1}. The inset shows the linear dependence of reduction peak currents on the glucose concentrations.

pulse amperometry (DPV) measurements were performed in PBS buffer (pH7.0) in the voltage range from −0.3 to −0.6 V (Fig. 5A). The sharp and well-defined reduction peak currents increased with the successive addition of glucose. At the same time, the reduction potential remained steady. The calibration curve fitted to determine the relationship between the peak current and the concentration of glucose was described by Ipa (μA)=3.02+1.37 C (mM) in the concentration range of 0–17 mM with R^2=0.990, and the sensitivity was 19.50 μA mM^{-1} cm^{-2}. These results were superior to other reported graphene and CNTs based electrodes, such as 0.01–6.5 mM and 7.95 μA mM^{-1} cm^{-2} for GOD on ERGO–MWCNTs hybrid modified GCE [36], 0.05–1.1 mM and 3.1 μA mM^{-1} cm^{-2} for GOD on Ag–polydopamine(Pdop)@CNTs nanocomposite modified GCE [47], and 2.0–16 mM and 1.76 μA mM^{-1} cm^{-2} for GOD on graphene–CdS nanocomposite modified GCE [48]. The comparison was summarized in Table 1. The PUCNT/GOD/GCE exhibited a wider linear range and an even higher sensitivity, indicating that the obtained electrode had excellent electrochemical activity. This excellent performance of the biosensor was attributed to large surface of the graphene pieces attached to the PUCNTs, the high electrical conductivity of PUCNTs from the inner CNTs, excellent biocompatibility of PUCNTs, and porosity of PUCNT/GCE, which enhanced the enzyme absorption on the electrode surface. Moreover, the prepared biosensor was fabricated by a facile and low cost procedure without expensive reagent and complicated experiment.

The apparent Michaelis–Menten constant (K_m) is a reflection of the enzymatic affinity, and an indicator of the enzyme–substrate reaction kinetics of a biosensor. K_m can be calculated using the Lineweaver–Burk equation [49]:

$$\frac{1}{I_{ss}} = \frac{K_m}{I_{max}}\frac{1}{C} + \frac{1}{I_{max}} \quad (4)$$

where C is the bulk concentration of the substrate, I_{ss} is the catalytic current (background current subtracted) in the steady state when the glucose concentration is C, and I_{max} is the maximum current measured under saturated substrate conditions. K_m of the PUCNT/GOD/GCE was calculated to be 5.09 mM. It was much smaller than values reported previously in the literatures, such as 6.7 mM at $(AuNPs/MWCNT)_5$/GOD/Au electrode [41], 11 mM at AuNP–SAMs–PNT/HRP–GOD [48] and 44.57 mM at CeO_2 NRs/GOx/ITO electrode [50] (summarized in Table 1). This lower value of K_m implied that the immobilized GOD had higher enzymatic activity, and that the PUCNT/GOD modified electrode exhibited a higher affinity for glucose.

3.4. Interference, stability and reproducibility

DA, UA and AA are coexisting electro-active species in real samples that can affect the response of a biosensor. To evaluate the anti-interference abilities of the electrode developed here, several coexisting compounds were selected (Fig. 5B). Only one clear peak could be observed for glucose in the presence of DA, AA, or UA alone, or a mixture of three. Both the peak potentials and the peak currents for glucose were fairly stable. These results demonstrated that the obtained biosensor had strong anti-interference abilities. The stability of the PUCNT/GOD/GCE was also investigated. After storing the electrode at 4 °C for three weeks, the response currents of the modified electrode retained 95% of its initial current, demonstrating that the PUCNT film provided a favorable microenvironment to retain the bioactivity of enzyme. Besides, the CV measurements on PUCNT/GOD/GCE were continuously scanned for 80 cycles and the response dropped by less 5%, revealing an acceptable stability of the electrode.

Furthermore, the reproducibility of the sensor measurements was investigated. Ten electrodes were fabricated and their responses

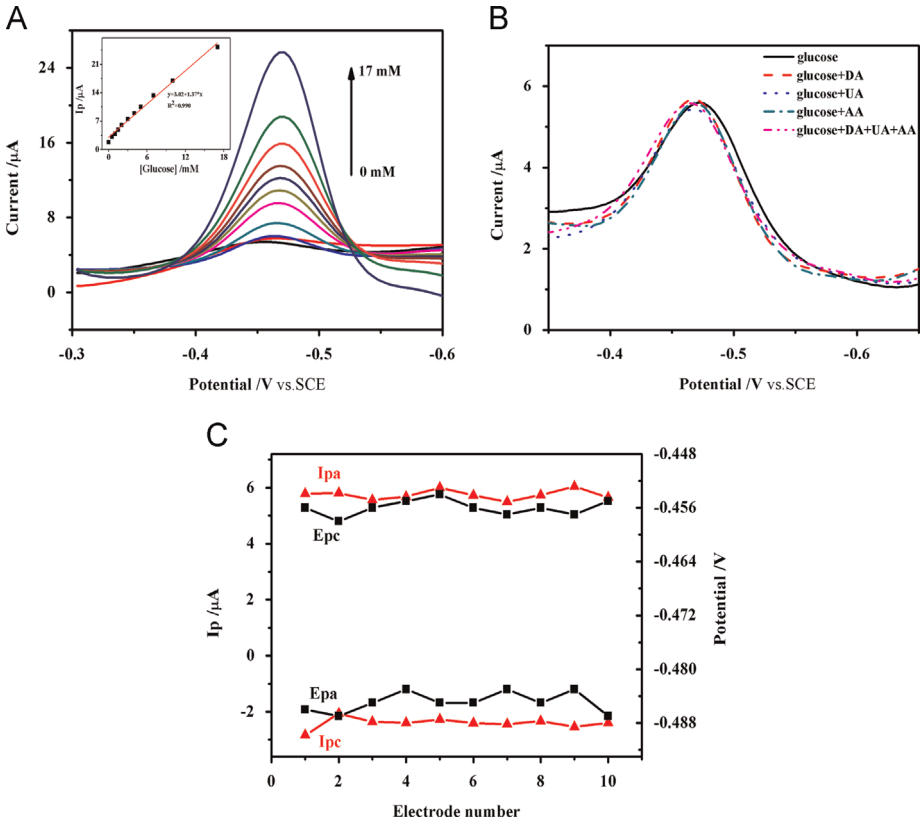

Fig. 5. (A) DPVs of PUCNT/GOD/GCE in O2-saturated PBS solution in various concentration of the glucose: 0, 0.5, 1, 1.5, 2, 3, 4, 5, 7, 10, and 17 mM. The inset is the linear dependence of peak currents on the glucose concentrations. (B) DPVs of PUCNT/GOD/GCE in 2 mM glucose solution, and glucose solution containing 1 mM DA, UA and AA respectively and 1 mM DA, UA, AA mixture (O_2-saturated 0.1 M PBS, pH7.0). (C) The current and potential responses of ten electrodes modified with PUCNT/GOD to 2 mM glucose.

Table 1
Comparison of selected electrochemical sensors for glucose detection.

Electrode	Linear range (mM)	Sensitivity ($\mu A\ mM^{-1}\ cm^{-2}$)	K_m (mM)	References
PUCNT/GOD	0–17	19.50	5.09	This work
SWCNHs[a]/Nafion/GOD	0–6	1.06	8.5	[51]
Nafion/Ag/Pdop@CNT/GOD	0.05–1.1	3.1	5.46	[47]
Graphene/CdS/GOD	2.0–16	1.76	1.6	[52]
Pt-CNTs/GOD	0.16–11.5	2.28	2.6	[53]
$(AuNPs/MWCNT)_5$/GOD/Au electrode	0.02–10	19.27	6.7	[41]
CNT/PTBO[b]/HRP[c]+GOD	0.1–1.2	0.113	33	[54]
Chitosan–ferronene/GO/GOD	0.02–6.78	10	2.1	[55]
Graphene/Chitosan/GOD	0.08–12	37.93	4.4	[56]
CS–Fc[d]/MWNTs/GOD	0.02–5.36	21.94	6.87	[57]
AuNP–SAMs–PNT/HRP-GOD[e]	0.5–2.4	4.29	11	[48]
CeO_2 NRs[f]/GOx/ITO electrode	2–26	0.165	44.57	[50]

[a] Single-walled carbon nanohorns.
[b] Poly(toluidine blue O).
[c] Horseradish peroxidase.
[d] Ferrocene-branched chitosan.
[e] Gold nanoparticle-self-assembled monolayers-peptide nanotube/horseradish peroxidase–GOD.
[f] CeO_2 nanorods.

to 2 mM glucose in O_2 saturated PBS (0.1 M, pH7.0) were measured under identical conditions (Fig. 5C). The relative standard deviation (RSD) of the *I*p was less 2% and the RSD of Ep was less 1%. These results showed that the fabrication procedure of the biosensor was reliable and that the modified electrodes were reproducible.

4. Conclusion

In the present work, a simple, low-cost, and efficient technique for the fabrication of a glucose biosensor was developed. By efficiently entrapping GOD in PUCNTs with high biocompatibility and good film-forming properties, the direct electrochemistry of GOD was achieved, and the immobilized GOD retained its bioactivity. The fabricated biosensor showed satisfactory analytical performance over a wide linear range from 0 to 17 mM, and a high sensitivity (19.50 $\mu A\ mM^{-1}\ cm^{-2}$); this was because of the large surface area and fast electron transfer of the PUCNTs. Interference from UA, AA, and DA was shown to be negligible, and the excellent stability was demonstrated. The excellent overall performance of this biosensor suggests that it has the potential to provide a new

platform for the fabrication of biocompatible glucose biosensors and other types of biosensors.

Acknowledgments

This research was supported by the National Natural Science Foundation of China (Nos. 51172045 and 51402051).

References

[1] R. Lv, E. Cruz-Silva, M. Terrones, ACS Nano 5 (2014) 4061–4069.
[2] Y. Li, W. Zhou, H. Wang, L. Xie, Y. Liang, F. Wei, J. Idrobo, S.J. Pennycook, H. Dai, Nat. Nanotechnol. 6 (2012) 394–400.
[3] F. Guinea, J. Herrero, J. González, Phys. Rev. B 79 (2009) 165434.
[4] Ž. Šljivančanin, Phys. Rev. B 84 (2011) 85421.
[5] B. Huang, Y. Son, G. Kim, W. Duan, J. Ihm, J. Am. Chem. Soc. 49 (2009) 17919–17925.
[6] X. Chen, Y. Xu, X. Zou, B. Gu, W. Duan, Phys. Rev. B 87 (2013) 155438.
[7] H. Santos, L. Chico, L. Brey, Phys. Rev. Lett. 103 (2009) 86801.
[8] D. Wei, L. Xie, K. Lee, Z. Hu, S. Tan, W. Chen, C. Sow, K. Chen, Y. Liu, A.T.S. Wee, Nat. Commun. 4 (2013) 1374–1378.
[9] L. Xie, H. Wang, C. Jin, X. Wang, L. Jiao, K. Suenaga, H. Dai, J. Am. Chem. Soc. 27 (2011) 10394–10397.
[10] L. Ye-Fei, B. Li, H. Zhang, Nanotechnology 22 (2009) 225202.
[11] Z. Yan, Z. Peng, G. Casillas, J. Lin, C. Xiang, H. Zhou, Y. Yang, G. Ruan, A.O. Raji, E.L.G. Samuel, R.H. Hauge, M.J. Yacaman, J.M. Tour, ACS Nano 5 (2014) 5061–5068.
[12] S. Costamagna, A. Schulz, L. Covaci, F. Peeters, Appl. Phys. Lett. 23 (2012) 232104.
[13] C. Sun, C. Chang, H. Lee, J. Zhou, J. Wang, T. Sham, W. Pong, ACS Nano 10 (2011) 7788–7795.
[14] D. Long, W. Li, W. Qiao, J. Miyawaki, S. Yoon, I. Mochida, L. Ling, Chem. Commun. 33 (2011) 9429–9431.
[15] A. Ambrosi, C.K. Chua, A. Bonanni, M. Pumera, Chem. Rev. 14 (2014) 7150–7188.
[16] D.A.C. Brownson, D.K. Kampouris, C.E. Banks, Chem. Soc. Rev. 21 (2012) 6944–6976.
[17] K.R. Ratinac, W. Yang, J.J. Gooding, P. Thordarson, F. Braet, Electroanalysis 4 (2011) 803–826.
[18] M. Pumera, A. Ambrosi, A. Bonanni, E.L.K. Chng, H.L. Poh, Trends Anal. Chem. 9 (2010) 954–965.
[19] R.L. McCreery, Chem. Rev. 7 (2008) 2646–2687.
[20] M. Pumera, Chem. Soc. Rev. 11 (2010) 4146–4157.
[21] M.F.L. De Volder, S.H. Tawfick, R.H. Baughman, A.J. Hart, Science 6119 (2013) 535–539.
[22] S. Park, M. Vosguerichian, Z. Bao, Nanoscale 5 (2013) 1727–1752.
[23] J. Wang, Electroanalysis 1 (2005) 7–14.
[24] H. Wang, Y. Wang, Z. Hu, X. Wang, ACS Appl. Mater. Interfaces 12 (2012) 6827–6834.
[25] G. Wang, Y. Ling, F. Qian, X. Yang, X. Liu, Y. Li, J. Power Sources 11 (2011) 5209–5214.
[26] X. Li, T. Li, Q. Zhong, K. Du, H. Li, J. Huang, Electrochim. Acta 125 (2014) 170–175.
[27] J. Li, B. Peng, G. Zhou, Z. Zhang, Y. Lai, M. Jia, ECS Electrochem. Lett. 2 (2013) A25–A27.
[28] J. Hernández-Ferrer, P. Laporta, F. Gutiérrez, M.D. Rubianes, G. Rivas, M.T. Martínez, Electrochem. Commun. 0 (2014) 26–29.
[29] L. Chen, M. Feng, H. Zhan, Electrochem. Commun. 48 (2014) 138–141.
[30] Y. Song, M. Feng, H. Zhan, Electrochem. Commun. 45 (2014) 95–98.
[31] F. Valentini, L.G. Fernàndez, E. Tamburri, G. Palleschi, Biosens. Bioelectron. 43 (2013) 75–78.
[32] G. Fu, X. Yue, Z. Dai, Biosens. Bioelectron. 9 (2011) 3973–3976.
[33] B. Liang, L. Fang, G. Yang, Y. Hu, X. Guo, X. Ye, Biosens. Bioelectron. 43 (2013) 131–136.
[34] H.D. Jang, S.K. Kim, H. Chang, K. Roh, J. Choi, J. Huang, Biosens. Bioelectron. 38 (2012) 184–188.
[35] B. Unnikrishnan, S. Palanisamy, S. Chen, Biosens. Bioelectron. 1 (2013) 70–75.
[36] V. Mani, B. Devadas, S. Chen, Biosens. Bioelectron. 41 (2013) 309–315.
[37] K. Hwa, B. Subramani, Biosens. Bioelectron. 62 (2014) 127–133.
[38] A.L. Higginbotham, D.V. Kosynkin, A. Sinitskii, Z. Sun, J.M. Tour, ACS Nano 4 (2010) 2059–2069.
[39] M. Pagán, D. Suazo, N. Del Toro, K. Griebenow, Biosens. Bioelectron. 62 (2015) 138–146.
[40] S.B. Bankar, M.V. Bule, R.S. Singhal, L. Ananthanarayan, Biotechnol. Adv. 4 (2009) 489–501.
[41] P. Si, P. Kannan, L. Guo, H. Son, D. Kim, Biosens. Bioelectron. 9 (2011) 3845–3851.
[42] J. Wang, Chem. Rev. 2 (2008) 814–825.
[43] Z. Yang, Y. Tang, J. Li, Y. Zhang, X. Hu, Biosens. Bioelectron. 54 (2014) 528–533.
[44] A.J. Bard, L.R. Faulkner, Electrochemical Methods: Fundamentals and Applications, 2nd ed, John Wiley & Sons, New York, 2001.
[45] J. Zhang, M. Feng, H. Tachikawa, Biosens. Bioelectron. 12 (2007) 3036–3041.
[46] Z. Yang, X. Huang, R. Zhang, J. Li, Q. Xu, X. Hu, Electrochim. Acta 70 (2012) 325–330.
[47] Y. Wang, L. Liu, M. Li, S. Xu, F. Gao, Biosens. Bioelectron. 1 (2011) 107–111.
[48] B. Park, R. Zheng, K. Ko, B.D. Cameron, D. Yoon, D. Kim, Biosens. Bioelectron. 1 (2012) 295–301.
[49] F.R. Shu, G.S. Wilson, Anal. Chem. 12 (1976) 1679–1686.
[50] D. Patil, N.Q. Dung, H. Jung, S.Y. Ahn, D.M. Jang, D. Kim, Biosens. Bioelectron. 1 (2012) 176–181.
[51] X. Liu, L. Shi, W. Niu, H. Li, G. Xu, Biosens. Bioelectron. 12 (2008) 1887–1890.
[52] K. Wang, Q. Liu, Q. Guan, J. Wu, H. Li, J. Yan, Biosens. Bioelectron. 5 (2011) 2252–2257.
[53] Z. Wen, S. Ci, J. Li, J. Phys. Chem. C 31 (2009) 13482–13487.
[54] W. Wang, F. Wang, Y. Yao, S. Hu, K. Shiu, Electrochim. Acta 23 (2010) 7055–7060.
[55] J. Qiu, J. Huang, R. Liang, Sens. Actuators B 1 (2011) 287–294.
[56] X. Kang, J. Wang, H. Wu, I.A. Aksay, J. Liu, Y. Lin, Biosens. Bioelectron. 4 (2009) 901–905.
[57] R. Liang, L. Fan, R. Wang, J. Qiu, Electroanalysis 15 (2009) 1685–1691.